RESEARCH: Original Research

Check for updates

Thermally drawn rechargeable battery fiber enables pervasive power

Tural Khudiyev [1,#], **Benjamin Grena** [1,2,#], **Gabriel Loke** [2], **Chong Hou** [3], **Hyeonji Jang** [4], **Jinhyuk Lee** [5], **Grace H. Noel** [6], **Juliette Alain** [2], **John Joannopoulos** [7,8], **Kang Xu** [9], **Ju Li** [2,5], **Yoel Fink** [1,2,5], **Jung Tae Lee** [4,*]

[1] Research Laboratory of Electronics, Massachusetts Institute of Technology, 77 Massachusetts Avenue, Cambridge, MA 02139, USA
[2] Department of Materials Science and Engineering, Massachusetts Institute of Technology, 77 Massachusetts Avenue, Cambridge, MA 02139, USA
[3] School of Optical and Electronic Information, Huazhong University of Science and Technology, Wuhan 430074, Hubei, China
[4] Department of Plant and Environmental New Resources, Kyung Hee University, Yongin 17104, Gyeonggi-do, Republic of Korea
[5] Department of Nuclear Science and Engineering, 77 Massachusetts Avenue, Cambridge, MA 02139, USA
[6] Department of Chemical Engineering, Massachusetts Institute of Technology, 77 Massachusetts Avenue, Cambridge, MA 02139, USA
[7] Department of Physics, 77 Massachusetts Avenue, Cambridge, MA 02139, USA
[8] Institute for Soldier Nanotechnologies, Massachusetts Institute of Technology, 77 Massachusetts Avenue, Cambridge, MA 02139, USA
[9] Electrochemistry Branch, Sensor and Electron Directorate, U.S. Army Research Laboratory, 2800 Powder Mill Road, Adelphi, MD 20783, USA

The increasing demand for mobile computing, communications, and robotics presents a growing need for suitable portable power solutions in non-flat customized electronic devices. Fibers as fundamental building blocks of fabrics and 3D-printed objects provide unique opportunities for developing pervasive multidimensional power systems. The characteristic small diameter ($<10^{-3}$ m) and high aspect ratios ($>10^6$) of fibers and expansion of fibers into 2D and 3D power systems necessitate ultra-long lengths to meet the energy specifications of portable electronic systems. Here, we present a Li-ion battery fiber, fabricated for the first time using a thermal drawing method which occurs with simultaneous flows of multiple complex electroactive gels, particles, and polymers within protective flexible cladding. This top-down approach allows for the production of fully-functional and arbitrarily long lithium-ion fiber batteries. The continuous 140 m fiber battery demonstrates a discharge capacity of ∼123 mAh and discharge energy of ∼217 mWh. The scalability and material tunability of these fibers position them for use in varied non-planar electronic systems, including a 1D-flexible electronic fiber, a 2D-large-scale machine woven electronic fabric (∼1.6 m^2), and a 3D-printed structural electronic system. The fiber battery satisfies the requirements of portable electronics systems as it is machine washable, flexible, usable underwater, and fire/rupture-safe. We have demonstrated the powering of a submarine drone, LiFi fabric, and flying drone communication through different rechargeable fiber battery schemes, which paves the way for the emergence of the pervasive battery-powered electronics.

Keywords: Li-ion battery; Ultra-long fiber battery; Multimaterial thermal drawing; Fabric electronics; 3D printing

---

Introduction

Innovation in the form factor of electronics continues to push the limits of applications for electronic systems. Currently, advanced battery-powered electronics can be foldable, flexible, and rollable but the battery component is still rigid and bulky. Unconventional batteries that would be mechanically flexible, compact, and mass-produced without sacrificing energy storage capabilities are needed for the realization of innovative electronics in new form factors. Fibers offer a unique platform for building these advanced compliant power systems in a bottom-up manner. They are ubiquitous and fundamental building blocks in our daily life; we find them in fabrics we wear, in the vehicles we drive, and in the homes we live in. Long lengths of fibers can be integrated into two-dimensional fabrics or be the feeding material to construct three-dimensional objects. These opportunities motivate the development of a fiber battery that can power a large suite of non-planar electronics of varying architectures spanning from 1D to 3D power sources.

The goal of realizing energy storage in fibers has been the focus of a number of previous publications [1–9]. The small diameter ($<10^{-3}$ m) of fibers requires extended fiber battery lengths ($>10^2$ m) in order to provide similar capacities to conventional batteries. However, outstanding fundamental challenges have limited the lengths of the functional fiber devices from previous works to the centimeter-scale [10]. Reliable fiber battery fabrication should involve materials and an architecture that promote fast ionic transport in the transverse direction and electronic transport in the axial direction so that the electrochemical performance is not hindered at narrow fiber thicknesses or long fiber lengths. In the transverse direction, the presence of interfacial gaps, especially between the electrolyte and electrode, reduces the rate of ionic transport across the fiber. The use of carbon-active material composites as electrodes in previous work lead to high electronic resistance in the axial direction, causing the length-normalized performance to decrease as fiber length increases [10]. In addition, the fiber battery should exhibit environmental stability, water resistance, and robust meachanical properties in order to realize its variety of applications.

The preform-to-fiber thermal drawing approach for fiber production stands out as an intrinsically scalable fabrication method – with more than 100 million kilometers of optical fiber produced every year using the same method [11]– while offering the ability to combine multiple materials into complex fiber architectures [12–23]. In this method, the constituent materials are assembled into a preform of the desired architecture. The cross-sectional geometry of the preform is preserved as it is heated above its melting point and scaled down into fiber. Recently, an ultra-long electric double layer capacitor (EDLC) fiber with promising electrochemical performance was successfully prepared by thermal drawing of multiple gels [22]. Although EDLC enables high power densities, the energy storage mechanism, which is based on the physical separation of charges, results in inherently low energy densities. Therefore, the use of battery fiber is preferred in situations where high energy densities are needed. Thermal drawing of battery components presents a unique set of challenges. In order to achieve laminar flow so that the cross-section geometry is preserved during the preform to fiber transition, the materials must be carefully selected to have similar viscosities that allow them to flow without mixing. The rheological and thermomechanical properties of active battery materials do not initially appear to be compatible with thermal drawing. For example, commonly produced composite-based electrodes have high particle loadings that increase viscosity and thus inhibit flow. Even with a low-viscosity electrode material, co-flowing all the components of a battery while maintaining physical separation of anode and cathode and guaranteeing intimate contact of both electrodes with the electrolyte is a significant challenge. Furthermore, typical battery active materials either have very high melting points or degrade prior to melting. Lastly, high-temperature processing could trigger chemical reactions and material degradation that would render the battery electrochemically deactivated.

This study describes how these challenges are addressed to produce the first thermally-drawn Li-ion fiber battery which is fully operational across hundreds of meters to power multiple electronics in new form factors. Three different gel components in which each gel is composed of four to six different materials are drawn to achieve segregated domains of anode, cathode, and electrolyte (Fig. 1). The gels are prepared via thermally-induced phase separation (TIPS) whereby the PVDF matrix solidifies from the EC:PC solvent [24]. TIPS is a well-known procedure for producing interconnected porous structures based on the temperature-dependent solubility of the polymer [25,26]. At an elevated temperature, a homogenous polymer solution is formed, and the polymer and solvent separate upon cooling. The thermal drawing method enables interfacial bonding with minimal gaps between the different domains over the entire length of the fiber as the domains interface in the liquid phase during the draw. Also, the thermally drawn fiber battery incorporates metallic microwires integrated into a conductive polymer in order to preserve axial conductivity while achieving structural integrity and full contact of battery electrode with the current collector. The fiber battery is then utilized for the realization of compliant power sources from 1D to 3D via bottom-up approaches (*i.e.* fiber-drawing, machine weaving, 3D printing) (Fig. 1). This approach introduces the concept of a pervasive fiber battery for next-generation mobile electronics.

Results and discussion

Gel-based electrodes and an electrolyte with tunable rheological properties are developed to be compatible with the thermal drawing process. To make the electrodes, polyvinylidene fluoride (PVDF) is mixed with active materials: lithium–iron-phosphate (LFP) as the cathode and lithium titanate (LTO) as the anode plus additional carbon black for electrical conductivity. This study employs LFP cathodes and LTO anodes in the fiber battery system because they are commercially available for mass production, show flat voltage plateaus for facile interpretation of electrochemical behaviors, and have signature elements to aid in visually observing any material mixture after fiber drawing via elemental analysis. The mixtures are solvated with a non-aqueous electrolyte consisting of 1 M bis(trifluoromethane)sulfo
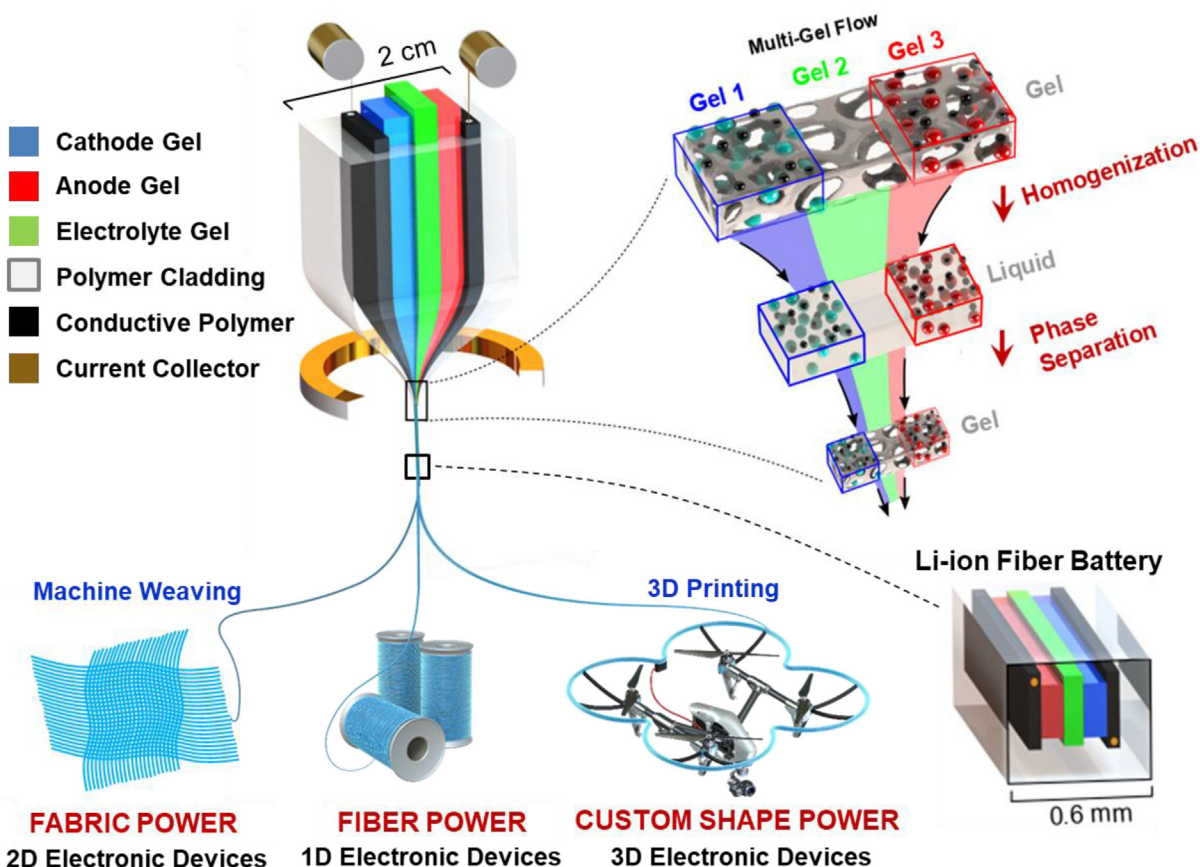
FIGURE 1

Thermal fiber battery drawing including multiple gels and its expansion into 2D and 3D flexible multidimensional electronics. The thermally drawn fiber battery consists of lithium–iron-phosphate (LFP) gel for the cathode, lithium titanate (LTO) gel for the anode, electrolyte gel, cyclic olefin copolymer (COC) cladding, and metal wires embedded in carbon-loaded polyethylene (CPE). The PVDF and EC:PC solvent mixture in LFP, LTO, and electrolyte gels are homogenized at the elevated temperature (in the furnace) and then phase-separated at room temperature (outside the furnace) forming interconnected pore structures with minimal gaps between cathode, anode, and electrolyte. The fiber battery can be integrated with electronic components to form 1D, 2D, and 3D electronic devices.

nimide lithium salt (LiTFSI) in ethylene carbonate (EC)/propylene carbonate (PC) (1:1 by volume) solution at 200 °C. The electrolyte is made similarly with PVDF in 1 M LiTFSI in EC:PC solution. At high temperatures, the solvents dissolve the polymer and the electrode and electrolyte assemblies become viscous liquids, but at room temperature, these gels behave as rubbery solids (Fig. S1). We confirmed the electrochemical activity of our gels by assembling half cells and full cells using molded anode, cathode, and electrolyte gels. The cells demonstrate similar cycling behaviors as previously reported for those electrode chemistries, thus proving that these materials remain fully functional after the heat treatment [27,28] (Figs. S2 and S3).

By selecting the appropriate ratio of polymer, solvent, and particulate materials, the viscosity of the electrode and electrolyte gels are tuned such that they become drawable at the draw temperature of 200 °C and maintain mechanical integrity at low temperatures. For a functional fiber battery, the precise placement of materials with strict separation is crucial. Local mixing between anode and cathode at any point along the fiber results in a short-circuit and renders the whole fiber length inactive. The internal convective mixing during thermal drawing can

be avoided only when all three gels have similar viscosities (Fig. S4). The electrochemical gels in the resulting fibers should also be bonded to one another because gaps significantly hinder ionic transport. This is achieved through viscoelastic fluid–fluid consolidation. During thermal drawing, the electrolyte and electrode gels melt to form viscoelastic liquids, which flow to fill any gaps present at their interface. Upon exiting the hot zone, the liquids within the fiber then solidify to form gels with a seamless interface with minimal gaps. Unlike conventional bottom-up approaches where gel electrolyte coated electrode fibers are twisted or stacked in parallel, this method allows for fluid phase consolidation to uniquely enable efficient bonding for fast ionic transport, and reduce the likelihood of defects. Furthermore, the common PVDF base for the different components (cathode, anode, and electrolyte) enhances the stability of the drawing process and promotes adhesion between the different domains in the resulting fiber.

In addition to the electrode and electrolyte gels, the macroscopic preform consists of cladding and current collectors. The preform is made from cyclic olefin copolymer (COC) and two carbon-loaded polyethylene (CPE) sheets and contains a channel

for the active components to be inserted before the draw. The COC cladding fully encases the fiber components during the draw, providing stability, moisture-resistance, and safety in the resulting fiber. The current collectors consist of two CPE layers, each with a small hole for a metal wire to be fed through during the draw. This current collector design enables high surface-area contact from the CPE layers, high axial conductivity from the metal wires, and structural stability of fiber during the draw. The wires are made of either tungsten or copper and have a diameter of 50 or 100 μm. Both of these metals offer high conductivity, and the use of either demonstrates the tunability of the system. The metal wires without CPE would easily penetrate into the gel electrode, damaging the internal structure of fiber battery during the draw. Molded and precut anode, cathode, and electrolyte gels are then inserted into the channel and the top of

the preform is sealed, without blocking the holes on CPE, in an argon-glovebox. The preform is then heated around 200 °C and fed with tungsten or copper wires in a draw tower furnace under constant nitrogen gas purge, and it is scaled down into a fiber with a *draw down ratio* (ratio of preform cross-section dimensions to fiber cross-section dimensions) of approximately 30 (Fig. 1 and Fig. S5). The longest fully functional Li-ion fiber battery acquired in this study is ~140 meters, demonstrating the possibility of fiber battery mass production (Fig. S6).

The materials' distribution in the axial direction of the produced fiber was first assessed using an optical microscope. Fig. 2a and Fig. S7 show a side view and cross-sectional view, respectively, of a fiber battery sample where the LTO-anode and LFP-cathode are separated by the transparent electrolyte. Particle segregation is also confirmed via an energy dispersive
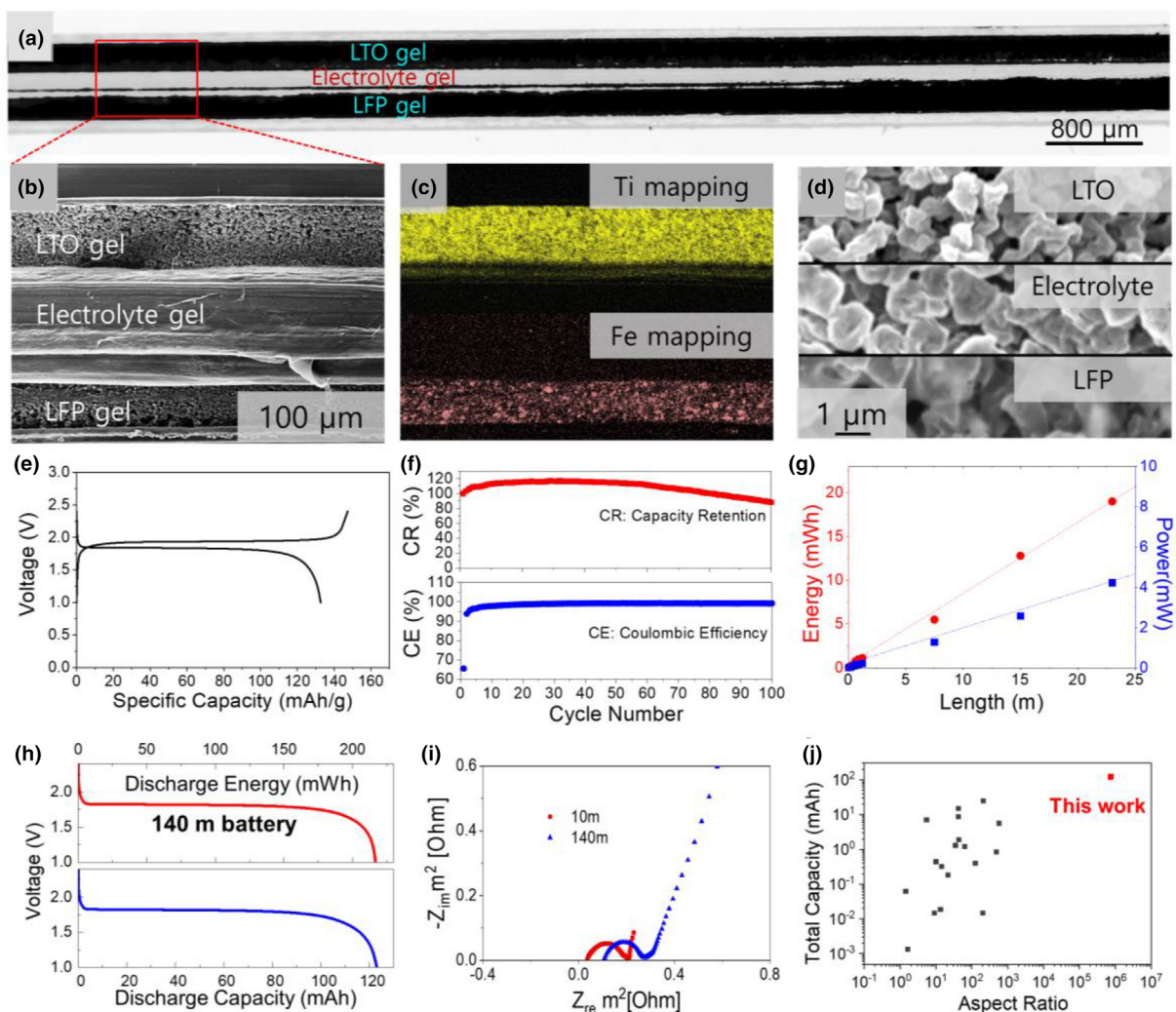

FIGURE 2

Morphology and electrochemical characterization of the fiber battery; (a) Optical micrograph of the side view showing clear segregations between anode and cathode, (b) SEM micrograph of dried fiber battery, (c) EDS Fe mapping and Ti mapping, (d) dried LFP, LTO, and electrolyte gels in fiber. SEM and EDS images are acquired after dissolving cladding material in cyclohexane under ambient conditions, (e) representative galvanostatic charge–discharge profile at ~C/5, (f) capacity retention and coulombic efficiency versus cycle number at ~5 C, (g) energy and power versus length of fibers. The cross-section area of active material is approximately 120(t) × 180(w) μm², (h) discharge profiles of 140 m thermally drawn battery fiber. (i) Nyquist plots of 10 m and 140 m battery fibers, and (j) total capacity vs aspect ratio of thermally drawn Li-ion battery fibers compared with previously reported fiber cells. For a cylindrical shape fiber, the diameter was used while for the ribbon shaped fiber, the averaged value of width and thickness (width + thickness/2) was adopted to calculate the aspect ratio.

spectroscopy (EDS) scan for titanium and iron, the signature elements of LTO, and LFP respectively (Fig. 2c). Scanning electron microscopy (SEM) further reveals the microstructure of dried battery gel components (Fig. 2d). Both electrodes and electrolyte display a highly porous solid framework, which results from the phase separation of the PVDF and mixed solvents at low temperatures. Minor microstructural differences between LTO- and LFP-electrodes are likely due to morphological differences in the original particles (Fig. S8). This porosity in the electrodes allows the Li$^+$ to access the active materials more easily, especially in thick electrodes [29], and the porous microstructure also permits high ionic transport flux between the electrolyte and electrodes [30–31].

In addition to microstructural characterization, electrochemical measurements were performed on thermally-drawn fiber battery samples. Fig. 2e shows the representative charge–discharge profiles of a LFP-LTO fiber battery from 1.0 V to 2.4 V at a 1 µA cm^{-1} rate (∼C/5). The fiber battery exhibits clear charge–discharge plateaus, with a lower voltage hysteresis for the fiber battery than the coin-cell configuration (Fig. S3c). This is because the LTO and LFP electrodes in the fiber battery are thinner than the electrodes used in the coin cell (∼120 vs. 500 µm), thus they are subject to a reduced internal resistance. The differential capacity plot shows sharp charge and discharge peaks at 1.94 V and 1.84 V, close to typical redox potentials for the LTO/LFP chemistry [27,32] (Fig. S9). The fiber batteries show nearly 90% capacity retention over 100 cycles with a Coulombic efficiency (CE) of ∼99% at a relatively fast rate of 5 C (25 µA cm^{-1}) (Fig. 2f). The initial CE is low compared with conventional Li-ion battery systems. The initial CE of the all-gel battery in coin cell is ∼93% and becomes higher than 99% (Fig. S3), meaning that the materials are in good condition before fiber drawing. However, the initial CE is low after fiber drawing due to air/moisture contamination during the draw. The initial CE is only 0.07% if the fiber is drawn under ambient atmosphere. However, this CE dramatically increases after minimizing air/moisture in the draw tower (Fig. S10). The initial CE can be further increased by thermal drawing under a more controlled environment. The absolute energy and power output of fiber batteries linearly increases as the length of the fiber increases, due to higher active material loading, without sacrificing performance (Fig. 2g). On average, the fiber cells exhibited length-normalized specific discharge energy of 9.6 (±1.4) µWh/cm and a length-normalized power density of 1.9 (±0.4) µW/cm. Balancing the N/P ratio is important in the full cell. Typically the N/P ratio is in the range between 1.03 and 1.2 for commercial Li ion batteries [33]. The N/P ratio can be easily balanced in the thermal drawing process by controlling the dimensions of the cathode and anode channels. In this study, the N/P ratio is ∼1.03 based on the theoretical capacities.

The current fiber battery design is not fully optimized, and the energy and power values could be further increased by increasing the amount of active materials per unit volume of cathode/anode gel or by increasing the amount of active gels per unit fiber. The PVDF fraction in the LFP and LTO electrodes is significantly larger than that in conventional electrodes. Less PVDF increases the energy density of fiber battery, but it decreases the viscosity of electrodes at the draw temperature, potentially rendering the

electrode structure unstable during the draw. To decrease the fraction of PVDF, future work can be done to formulate the electrodes with more active materials and less solvent to increase the viscosity for both stable drawing and high energy density. The 140-m long (Fig. 2h) fully-functional fiber battery demonstrates a discharge capacity of 123 mAh (8.8 µAh/cm) and discharge energy of 217 mWh (15.5 µWh/cm), which is sufficient to power a wide range of applications such as wearable devices, consumer products, and medical devices. This 140-m long fiber's length normalized capacity and energy values are increased ∼70% compared with the fibers used in Fig. 2e-f by introducing more active materials in the cathode and anode gels. The electrochemical impedance spectroscopy studies on 10-m and 140-m fiber batteries clearly show almost identical charge-transfer resistances, indicating stable fiber drawing and invariant battery microstructures along the fiber length (Fig. 2i). The theoretical voltage drop calculation [34] indicates the Cu micro-wires in a fiber battery create negligible potential drop for the 140 m long fiber battery (Fig. S11). Another advantage of the thermal drawing process is that the fiber's transverse dimensions can be controlled by changing the capstan speed without changing the preform (Fig. S12). For a conventional battery system, the technology and practice of producing and assembling ultra-long planar electrodes are well-developed. As a result, reporting normalized capacity (i.e. specific capacity) is sufficient to quantify device performance. However, for fiber devices, fabrication itself is challenging and the discrepancy of normalized capacities (i.e. length-normalized capacity) between short fibers and long fibers generally becomes larger as fiber length increases. Here, we introduce "total capacity" with respect to the aspect ratio of the device which is a new and key figure of merit in fiber-shaped batteries. Comparison of capacities between different active materials is rarely done for the fair comparison because each material has different theoretical capacities. However, the thermally drawn LIB fiber has the highest total capacity and aspect ratio compared to fiber batteries prepared via conventional approaches regardless of battery chemistry [1–2,7,35–49] (Fig. 2j).

The thermally drawn fiber battery with linearly preserved performance over long lengths enables pervasive power as it can be assembled into an electronic system of any desired dimensions and form factor via a bottom-up approach. The one-dimensional fiber battery is the direct output of fiber drawing for scalable power sources and is demonstrated in two applications. First, the integrated fiber that includes the electronics and the power source in the same fiber enables navigating to inaccessible regions, for example, monitoring and delivering functions to narrow lumens of the body or civil infrastructures. LEDs and battery components are co-drawn in the same 10-meter-long fiber with a 1.2 mm × 1.2 mm cross-sectional area, demonstrating the ability of the thermal drawing method to fabricate multifunctional fibers (Fig. 3 and Movie 1). Both the discrete LED microchips and battery fiber are encapsulated by elastomeric COC, during the preform to fiber transition, to enable a more flexible and soft fiber device (Fig. 3a). The connection between battery and LED is achieved using in-fiber terminals and this shows the unique capability of 1D power source in tetherless fiber devices. Second, a submarine drone is powered by a 20-meter-long fiber battery attached onto the curved surface
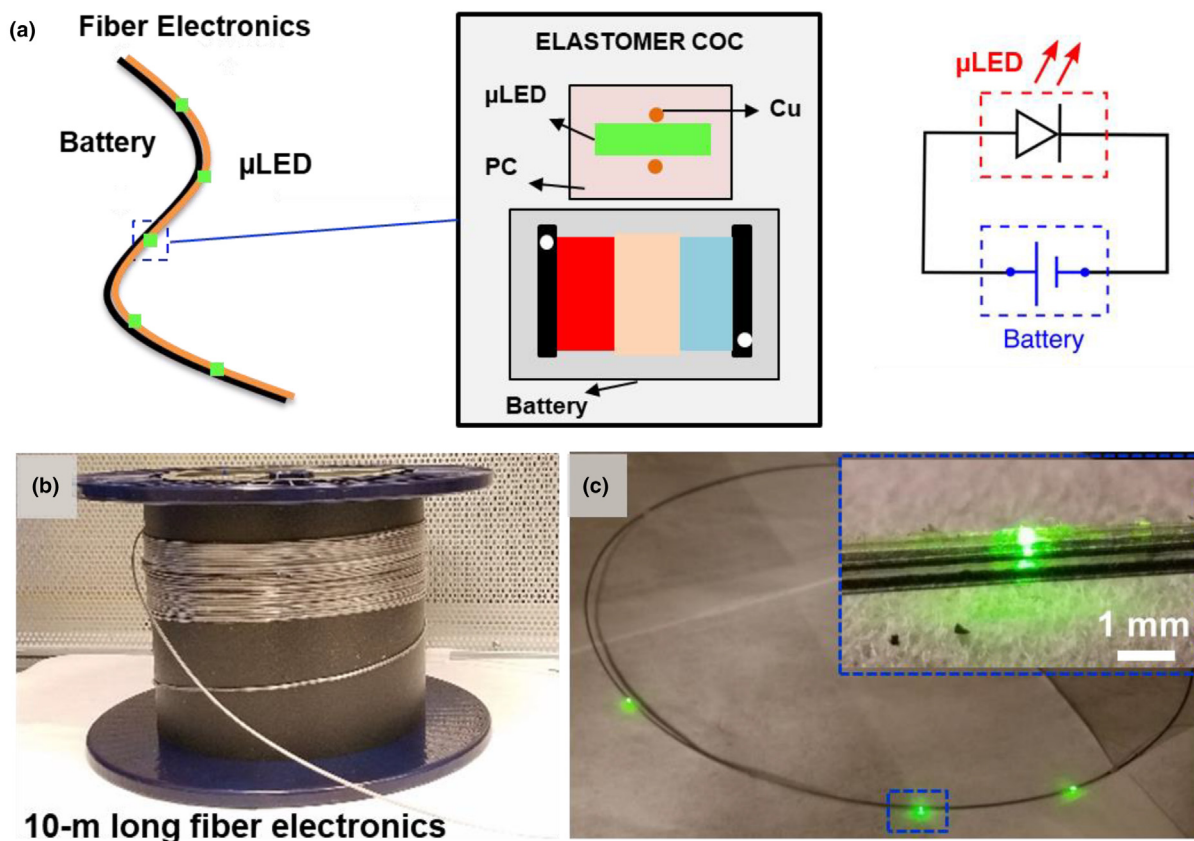
FIGURE 3

Thermally drawn fiber battery in 1D electronics; Integrated fiber battery through co-drawing of LED and battery modalities; (a) schematic diagram of integrated LED/battery fiber and its corresponding electrical circuit, (b) the 10-meter-long LED/battery fiber, (c) green LEDs powered by fiber battery within the same fiber.

(Fig. S13 and Movie 2). This demonstration shows the conformal attachment of the fiber to a non-flat surface, underwater resistance of the long fiber battery, and the ability to power an underwater drone while forming part of its structure (Movie 3).

The dimensional similarity and material compatibility of traditional yarns and the fiber battery facilitate its integration into 2D fabric electronics through machine weaving. A secondary elastomeric COC cladding is added to the battery design shown in Fig. 4a, and a 100-m long fiber battery is drawn with soft and flexible features. The battery fibers are woven into the large-scale textile (135×120 cm^2) via a conventional automated weaving machine (Fig. 4a and Fig. S14), demonstrating the promise of next-generation wearable electronics. The large-scale format of the thermally drawn fiber battery enables the powering of a suite of fabric electronics. By using the fiber battery as a unit block in smart textiles, the capacity and the voltage of the textile battery pack can be controlled by connecting fibers in series or parallel. For example, the capacity becomes triples when three fibers are connected in parallel, and the voltage doubles when two fibers are connected in series (Fig. 4b). Therefore, the capacity and voltage of battery arrays can be freely adjusted for specific applications.

Unlike traditional batteries that are restricted to rigid architectures, the fiber batteries are intended to be used in applications that experience mechanical deformations during regular use. Hence, the fiber battery should have robust mechanical properties without sacrificing electrochemical performance. Multiple experimental results corroborate the reliability of the thermally drawn fiber battery without appreciable change in the electrochemical behaviors. The thermally drawn battery fibers can sustain maximum tensile stress of ~33 MPa with a failure strain of ~34% (Fig. 4c). As tensile stress gets larger than ~27 MPa, the anode is in contact with the cathode resulting in failure of electrochemical functionality. After 1000 cycles of repeated mechanical bending, 96% of the initial capacity was retained over 30 charge–discharge cycles (Fig. 4d). The fibers continue to power an LED during combinations of dynamic bending and twisting (Movie 4). Furthermore, the thermally drawn fiber battery demonstrates nearly identical electrochemical performance after ten cycles of machine washing (Fig. 4d, and Movie 5). When fiber batteries are adopted in wearable devices, the battery is very close to if not in direct contact with the human body. As a result, the safety of the fiber battery under harsh conditions is even more important than it is for other conventional battery systems. The fiber battery continues to power an LED even after partial cutting, indicating that the fiber battery system is free from electrolyte loss, at least in the short-term, and from short-circuiting. (Fig. S15a, and Movie 6) Lastly, the thermally-drawn fiber battery is fire-resistant due to the gel electrodes and gel electrolyte whereas the control fiber battery with liquid electrolyte instantly catches fire and expands (Fig. S15b, and Movie 7).
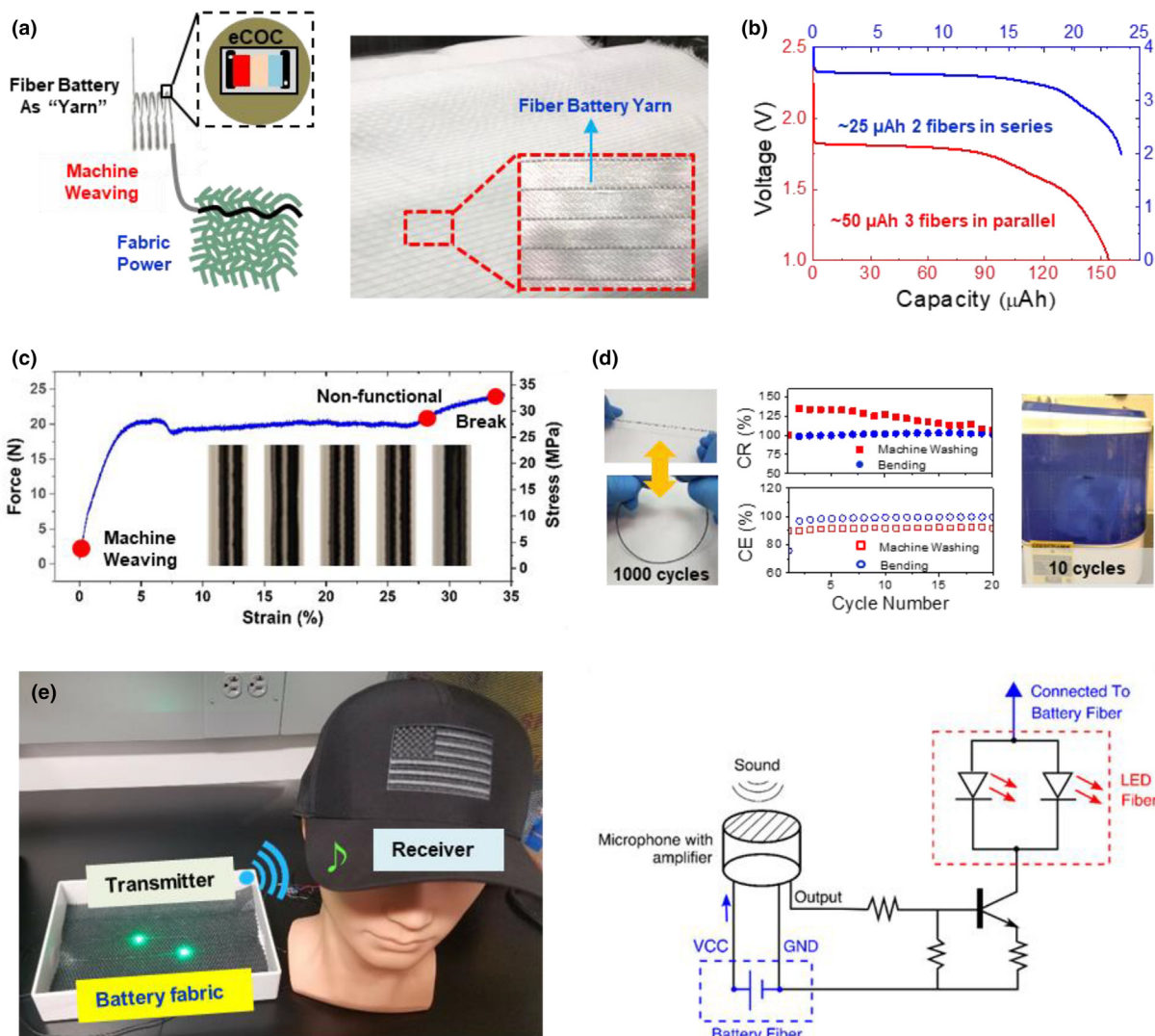
FIGURE 4

Thermally drawn fiber battery in 2D electronics; (a) A battery fiber embedded within 135 × 120 cm² textile. The 1.27 cm space between black fiber batteries is filled by white polypropylene coated glass fibers. The fiber battery powers flexible fiber-based fabric electronics. (b) Fiber battery in parallel and series configurations. Discharge profiles of three ~50 μAh fiber batteries in parallel and two ~25 μAh fiber batteries in series. (c) Force/Stress-Strain curve of a thermally drawn Li-ion fiber battery and side-view images of fiber battery corresponding to the strains of 10, 15, 20, 25, and 30%. (d) Capacity retentions after 1000 bending cycles and 10 washing cycles. (e) A 100 m long fiber battery-powered LiFi fabric sample as a next-generation communication fabric and its corresponding electric circuit. Fiber battery powers a microphone with a pre-amplifier, a transistor, and diode fibers.

Fiber batteries can be combined with additional in-fiber functionalities. We demonstrate a full system integration by producing a 100-m fiber battery which is used to power a fabric containing a microphone with a pre-amplifier, a transistor, and diodes (Fig. 4e, and Movie 8). Using light modulation, a fiber containing photodiodes can receive an audio signal optically and transform the signal back to the electrical domain. The received electrical output signal is fed to a receiver that can output to the speaker. This circuit demonstrates an analog optical transmission of audio, but the bandwidth of the LEDs can easily allow digital transmission of data in the MHz range, which would allow for protocols such as LiFi. Powering such a fabric communication system holds promise for next-generation human–computer interactions.

The scalability of the thermal drawing process and the material tunability of the fiber permits the usage of battery fibers as a modified print filament to form 3D energy storage structures. 3D-printed structures made from battery filament could take on customized shapes with energy storage capabilities. Printing the individual material components of a Li-ion battery is complex, but this challenge is resolved by printing a fiber that already contains all of these components. In a single thermal draw process, hundreds of meters of battery fiber with a printable poly-caprolactone (PCL) secondary cladding surrounding the COC primary cladding are produced (Fig. 5a). Key to the printability of these battery fibers is the presence of a thermally graded cladding structure, in which the glass transition temperature increases from the outer PCL cladding to the inner COC clad-
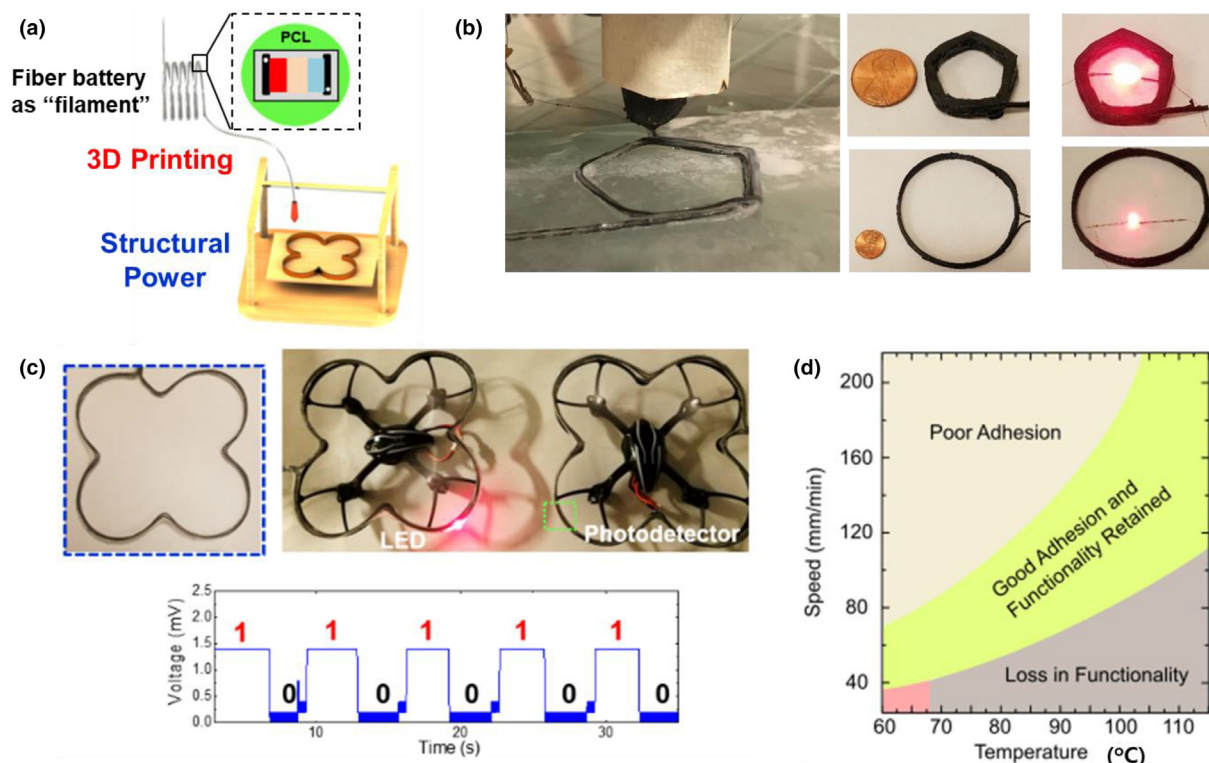
FIGURE 5

Thermally drawn fiber battery in 3D electronics; (a) Schematic diagram of 3D printing process by using a thermally drawn Li-ion battery fiber. Fiber battery with PCL cladding enables a new fiber battery direction towards 3D structural power, (b) multiple 3D-printed batteries in different shapes and size, (c) 3D-printed drone casings from the fiber battery. The 3D-printed drone casing powers the fiber LED, and photodetector system for drone-to-drone communication. (d) 3D product quality with respect to the 3D printing speed and temperature.

ding. At the print temperature, the PCL cladding melts and fuses with adjacent printed fibers, while the COC material remains at its solid-state, protecting the internal battery domain from inter-mixing and deformation during printing. The ability to cus-tomize battery structures is important in mobile systems, where weight must be minimized while ensuring sufficient energy to power the moving electronic device. To this end, the battery fiber is printed into multiple shapes including the external casing of a flying drone (Fig. 5b-c). Communication from the light-emitting diode of one drone to the photodiode of another drone is demonstrated with the LED and the photodiode powered by the printed battery casings (Fig. 5c and Movie 9). The quality of 3D printed battery is greatly affected by both temperature and speed of printing. (Fig. 5d). The printing of battery filaments should be carried out under sufficiently high temperature to fuse filaments but not too high as to prevent structural damage. The speed of printing is related to the cooling of the battery filament as well as to the production yield. All of these demonstrations illustrate a new potential of fiber-based batteries, wherein battery systems can be printed into any desired shape.

In this study, thermally drawn Li-ion fiber batteries are intro-duced to provide power solutions in distinct emerging technolo-gies, including wearables and 3D printed objects. Even more applications will be possible in the future as the fiber materials, structure, and processing are advanced. In terms of materials, gel compositions can be optimized for higher energy and power densities while still being compatible with the thermal drawing

process. The active materials in the gels could also be replaced with next-generation battery materials with high energy densi-ties to satisfy the power requirements of emerging portable and flexible electronics systems. Furthermore, the gel composition offers unique interface contact, flexibility, and safety characteris-tics for fiber battery design. In the fiber structure, the electro-chemically inactive cladding materials should be minimized while still providing the protection to withstand mechanical damage, machine weaving, or repeated use. The distance between anode and cathode can be optimized to minimize the ion travel distance, but this distance should be long enough to prevent possible short-circuit. Advancing the fiber processing to increase the production rate to one kilometer or higher per hour will improve the cost-effectiveness. Improving control of the environment during fiber processing will yield high CE and long cycle life.

Conclusion

A 140-m long lithium-ion fiber battery was produced for the first time via preform-to-fiber thermal drawing to power multiple electronics in new form factors. To achieve this, thermally-drawable anode, cathode, and electrolyte gels were developed. These materials behave as rubbery solids at room temperature but are able to flow at the elevated temperature of the drawing process, while still maintaining electrochemical functionality once cooled. The energy and power of fiber batteries increase pro-portionally with fiber length without length-limited perfor-

mance, and they demonstrate a discharge capacity of ~123 mAh and discharge energy of ~217 mWh. This study also illustrates pervasive power solutions of these fiber batteries for multidimensional flexible electronics. The thermal drawing method allows for integrating LEDs and battery into a single fiber. Fiber batteries of long lengths are produced and woven into fabrics to power textile electronics. Lastly, 3D printing of fiber batteries is demonstrated for lightweight, structural power. Multi-functionality within a single fiber and multi-dimensionality from a single fiber will power a new generation of smart fiber, fabric, and 3D-object electronic systems.

Methods

Thermally drawable battery gels
The active materials—LFP for the cathode (MTI Corporation), LTO for the anode (MTI Corporation), carbon black (VWR), PVDF (Arkema Inc.) and 1 M LiTFSI in PC:EC (1:1, v:v)—were mixed at 200 °C in an argon-glovebox (<1 ppm of H_2O, Innovative Technologies) for electrochemically active gels. The ratio of active material: carbon black: PVDF was 55:10:35 by weight. The electrolyte gel was prepared by mixing PVDF and 1 M LiTFSI in PC:EC (1:1, v:v) at 200 °C. The hot gels are poured onto the glass substrate and flat films are produced in the glovebox.

Preform fabrication and fiber drawing
Flat fiber batteries are drawn from a macroscopic rectangular preform. The thickness/width and the length of the preform are ~2 cm and ~25 cm respectively. First, CPE and COC (Topas) cladding are consolidated with hot-press at 125 °C. Small channels are left in the CPE for copper (or tungsten) wires to fed through during the draw. The preform is transferred to the Ar glovebox, and the cathode, anode, and electrolyte gels are inserted into the preform. The open end of the preform used for gel insertion is sealed by polyimide tape and chemically resistant epoxy. The preform is drawn under nitrogen flow in a three-zone vertical tube furnace with a top-zone temperature of 90 °C, a middle-zone temperature of 200 °C, and a bottom-zone temperature of 60 °C. The fiber dimensions were monitored with laser-micrometers.

Electrochemical characterization
The fiber batteries were equilibrated for 24 h before the operation. The long fiber battery was cut to the desired length and sealed with paraffin wax inside an Ar glovebox. The metal wires on both sides of the battery fiber are exposed by cutting out the COC cladding with a scalpel. Once the metal wires are exposed, the Cu wires are coiled, and silver paste is applied to ensure electrical connection. The fiber batteries are cycled between 2.4 V and 1.0 V at 1 μA/cm or 25 μA/cm in galvanostatic mode using an Arbin battery test system (Arbin Instruments).

3D printing of fiber battery
We use the Rova3D multi-nozzle printer for the printing of the battery fiber. The nozzle is custom-made with a short (~0.3 mm) stainless steel hot end of the same diameter as the fiber. The hot end is heated by a nichrome wire and the temperature is measured using a VWR thermocouple. The key idea for this printing approach is to heat the outer PCL layer of the bat-tery fiber for surface adhesion between individual printed lines, while the functional domains internal to the fiber are still preserved in the solid-state so that the battery functionality can be well-retained during printing. The battery fiber is printed at a temperature of 70 °C and a speed of 80–90 mm/min with the ratio of depositing (z) speed to the xy translation speed kept at 1:1. A thin PCL film, glued to the print bed, is used to increase adhesion between the first layer of the printed drone casing to the print bed. The input layer height of the print is set as the diameter of the fiber. The 3D design of the drone casing is constructed in SolidWorks and later processed via Slic3r to create a gcode file. The gcode is then fed into the Pronterface Software, which communicates the required XYZ print positions of the drone casing to the printer.

Machine weaving of fiber battery
We have used an automated weaving machine, type Picanol Gamma 190 cm dobby-rapier loom, to weave the Li-ion battery fabric. The fabric is an 8-harness satin weave construction woven at 32 threads per inch in the weft direction and 57 threads per inch in the warp direction. In these fabrics, the warp material is 900 denier polypropylene covered glass fiber and the weft material (other than battery fiber) is also 900 denier polypropylene covered glass fiber. The size of the fabric is 135 × 120 cm^2 and the battery fibers are spaced every 1.27 cm between the white polypropylene covered glass fibers.

Competing financial interests
The authors declare no competing financial interest.

Data availability
The datasets in this work is available upon reasonable request.

CRediT authorship contribution statement
Tural Khudiyev: Conceptualization, Methodology, Investigation, Validation, Data curation, Writing – original draft. **Benjamin Grena:** Conceptualization, Methodology, Investigation, Writing – original draft. **Gabriel Loke:** Methodology, Investigation, Writing – review & editing. **Chong Hou:** Investigation, Writing – review & editing. **Hyeonji Jang:** Investigation, Writing – review & editing. **Jinhyuk Lee:** Investigation, Writing – review & editing. **Grace H. Noel:** Investigation, Writing – review & editing. **Juliette Alain:** Investigation, Writing – review & editing. **John Joannopoulos:** Conceptualization, Writing – review & editing. **Kang Xu:** Methodology, Writing – review & editing. **Ju Li:** Methodology, Writing – review & editing. **Yoel Fink:** Conceptualization, Supervision, Writing – review & editing. **Jung Tae Lee:** Conceptualization, Methodology, Investigation, Validation, Data curation, Supervision, Writing – original draft.

Declaration of Competing Interest
The authors declare that they have no known competing financial interests or personal relationships that could have appeared to influence the work reported in this paper.

Acknowledgments

Appendix A. Supplementary data

Supplementary data to this article can be found online at https://doi.org/10.1016/j.mattod.2021.11.020.

References

[1] Q. Chen et al., Adv. Energy Mater. 8 (19) (2018) 1800054.
[2] Y.H. Kwon et al., Adv. Mater. 24 (38) (2012) 5192–5197.
[3] J. Park et al., Adv. Mater. 27 (8) (2015) 1396–1401.
[4] H. Qu et al., Smart Mater. Struct. 24 (2) (2014) 025012.
[5] J. Ren et al., Adv. Mater. 25 (8) (2013) 1155–1159.
[6] H. Sun et al., Nat. Rev. Mater. 2 (6) (2017) 17023.
[7] M. Wang et al., Adv. Funct. Mater. 30 (3) (2020) 1905971.
[8] X. Yu et al., Nano Energy 2 (6) (2013) 1242–1248.
[9] J. Zhou et al., Adv. Mater. 31 (3) (2019) 1804439.
[10] M. Liao et al., Adv. Electron. Mater. 5 (1) (2019) 1800456.
[11] J. Ballato, P. Dragic, Int. J. Appl. Glass Sci. 7 (4) (2016) 413–422.
[12] M. Bayindir et al., Nature 431 (2004) 826–829.
[13] A. Canales et al., Nat. Biotechnol. 33 (3) (2015) 277–284.
[14] S.D. Hart et al., Science 296 (5567) (2002) 510–513.
[15] M. Rein et al., Nat. Commun. 7 (1) (2016) 12807.
[16] B. Temelkuran et al., Nature 420 (6916) (2002) 650–653.
[17] A.M. Stolyarov et al., Nat. Photonics 6 (4) (2012) 229–233.
[18] T. Khudiyev et al., Nat. Commun. 8 (1) (2017) 1435.
[19] B. Grena et al., Nat. Commun. 8 (1) (2017) 364.
[20] S. Egusa et al., Nat. Mater. 9 (8) (2010) 643–648.
[21] A.F. Abouraddy et al., Nat. Mater. 5 (7) (2006) 532–536.
[22] T. Khudiyev et al., Adv. Mater. 32 (49) (2020) 2004971.
[23] G. Loke et al., Nat. Commun. 10 (1) (2019) 4010.
[24] J.T. Lee et al., PNAS 117 (35) (2020) 21155–21161.
[25] M. Gu, et al., Desalination, 192 (1-3) (2006), 160–167.
[26] S. Rajabzadeh et al., Sep. Purif. Technol. 63 (2) (2008) 415–423.
[27] C. Sun et al., J. Am. Chem. Soc. 133 (7) (2011) 2132–2135.
[28] K. Sun et al., Adv. Mater. 25 (33) (2013) 4539–4543.
[29] N. Nitta et al., Mater. Today 18 (5) (2015) 252–264.
[30] Z. Jiang et al., Electrochim. Acta 42 (17) (1997) 2667–2677.
[31] K. Abraham et al., Chem. Mater. 9 (9) (1997) 1978–1988.
[32] W. Liu et al., Adv. Mater. 28 (18) (2016) 3578–3583.
[33] X. Wu et al., Front. Energy Res. 7 (2019) 65.
[34] F. Sorin et al., Opt. Express 18 (23) (2010) 24264–24275.
[35] X. Li et al., Adv. Mater. 31 (39) (2019) 1903852.
[36] W. Weng et al., Nano Lett. 14 (6) (2014) 3432–3438.
[37] Y. Huang et al., ACS Nano 11 (9) (2017) 8953–8961.
[38] Z. Wu et al., Small 14 (22) (2018) 1800414.
[39] Z. Jin et al., Energy Storage Mater. 13 (2018) 160–167.
[40] Y. Zhang et al., Angew. Chem. Int. Ed. 54 (38) (2015) 11177–11182.
[41] W.G. Chong et al., Adv. Funct. Mater. 27 (4) (2017) 1604815.
[42] R. Liu et al., Nano Energy 33 (2017) 325–333.
[43] S.H. Ha et al., J. Mater. Chem. A 6 (15) (2018) 6633–6641.
[44] H. Song et al., Carbon 147 (2019) 441–450.
[45] Y. Zeng et al., Adv. Mater. 29 (44) (2017) 1702698.
[46] J.-K. Kim et al., J. Mater. Chem. A 2 (6) (2014) 1774–1780.
[47] X. Fang et al., Adv. Mater. 28 (3) (2016) 491–496.
[48] Y. Wang et al., J. Mater. Chem. A 6 (23) (2018) 10813–10824.
[49] T. Hoshide et al., Nano Lett. 17 (6) (2017) 3543–3549.